

**High-throughput investigation of the formation of double spinels**

Journal:	<i>Journal of Materials Chemistry A</i>
Manuscript ID	TA-ART-09-2020-009200.R1
Article Type:	Paper
Date Submitted by the Author:	17-Nov-2020
Complete List of Authors:	Kocevski, Vancho; Los Alamos National Laboratory, Pílania, Ghanshyam; Los Alamos National Laboratory, Uberuaga, Blas; Los Alamos National Laboratory,

ARTICLE

High-throughput investigation of the formation of double spinels

Vancho Kocevski,^{*a} Ghanshyam Pilania,^a and Blas P. Uberuaga^aReceived 00th January 20xx,
Accepted 00th January 20xx

DOI: 10.1039/x0xx00000x

Spinel compounds, with the general chemical formula AB_2O_4 are a wide class of materials, where A and B can be a variety of cations, providing this structure with a great deal of functional flexibility and giving rise to its considerable scientific interest. Recently, a spinel with the general formula $ABB'O_4$ has been predicted, increasing the possible usability of the spinels due to the higher cation diversity in the so-called *double spinel* structure. Here, we use density functional theory calculations to predict if double spinels can be formed between experimentally synthesized normal and inverse single spinels. Our computations reveal that 49 double spinels have negative mixing enthalpies and are thus thermodynamically stable, with most of the stable compounds being formed from one of two distinct cation orderings. We show that the 17 different cations that form the different double spinels have a preferred site, tetrahedral or octahedral, except for Mn, Fe and Co which can occupy both sites interchangeably. We also study the relation between mixing enthalpies and cation-specific properties, as well as ways to classify the double spinels into distinct types and spinel groups depending on the cation ordering and cation oxidation states, respectively. By applying the Sure Independence Screening and Sparsifying Operator (SISSO) approach on the coordination-dependent ionic radii of the elemental constituents, we show that an interplay of local strain and electrostatic dominated terms can be used to separate the double spinels into distinct structural types depending on the cation order and their oxidation states.

Introduction

Since their discovery more than a century ago, spinel oxides have found their way into many aspects of science, technology and everyday life. Named after the mineral “spinel” ($MgAl_2O_4$), they can be found in igneous rocks and as metamorphic minerals, thus having considerable importance in petrological studies (1). Spinel has also been used as precious stones in jewelry due to their relatively high hardness and luscious colors that can span the whole visible spectrum as well as black. Possibly the single most important feature of spinels is their diversity in cation chemistries, coming from the fact that the synthesized spinels contain most of the main group and transition metals. Together with the fact that the cation chemistry significantly influences the properties of spinels, they exhibit a range of interesting electronic (2; 3), optical (4; 5), superconducting (6; 7), catalytic (8; 9; 10; 11; 12) and magnetic/multiferroic (13; 14; 15; 16; 17; 18; 19) properties, while changing cation chemistry allows for tailoring the properties to specific needs. This diversity of properties makes spinels useful in a variety of applications, such as energy storage (20; 21), sensing (22), lasers (23; 24), biotechnology (25), transparent conducting oxides (26; 27), data storage (28), dielectrics (29) and high frequency electronic devices (30).

Spinel compounds, typically represented by the formula AB_2O_4 , where the O ions form a cubic closed-packed sublattice and the A and B cations occupy $\frac{1}{8}$ of the tetrahedral and $\frac{1}{2}$ of the octahedral sites, respectively. This is the most commonly occurring spinel structure, termed “normal” and first characterized by Bragg (31; 32) and Nishikawa (33) in 1915. The normal spinel can also be represented as $(A)[B_2]O_4$, where the cation residing on the tetrahedral site is denoted with parenthesis while, with square brackets, the cation on the octahedral site is represented. In what follows, we will omit the square brackets, and only use the parenthesis to denote the cation in tetrahedral site for simplicity. Additionally, Barth and Posnjak (34) found that the cation ordering in the ground state of some spinels is reversed (inverse) from the normal, where the tetrahedral site is occupied by the B cation, while the octahedral sites are shared by the A and B cations, i.e., $(B)ABO_4$, termed an “inverse” spinel. At finite temperatures the cations on both tetrahedral and octahedral sites can start to mix, giving rise to an intermediate configuration $(A_{1-x}B_x)A_xB_{2-x}O_4$, where x denotes the degree of inversion. The degree of inversion ranges from 0 for normal spinel to 1 for inverse spinel, and $\frac{1}{3}$ for a completely random distribution of the cations. It has also been shown that binary solid solutions can be formed by mixing two single spinels of the same type, while mixing between normal and inverse spinels is generally considered to be unlikely (35). Interestingly, recently it was shown that an ordered quaternary spinel, $(Ga)MgAlO_4$, can be formed from normal and inverse spinels (36), despite this notion that normal and inverse spinel should not mix. This spinel was termed a “double” spinel as it can be considered a hybrid of the normal and inverse single spinels, inspired by the notation used for perovskites. At the same time, the same study showed that the two inverse spinels $(Ga)MgGaO_4$ and $(In)MgInO_4$ do not have a negative mixing energy and any mixing in that system would be driven by entropy alone. Other possible orderings of the octahedral sublattice have also been

^a Materials Science and Technology Division, Los Alamos National Laboratory, Los Alamos, NM 87545, USA.

* Corresponding author, email: kocevski@lanl.gov; Vancho.vk@gmail.com

Electronic Supplementary Information (ESI) available: Tables containing: energies of all single spinels used in the study, mixing enthalpies of all double spinels with the three different cation orderings, non-spinel phases stability and re-evaluated double spinel mixing enthalpies, relative stability of the Co containing single spinels. Figures showing: violin plots of cation properties of all double spinels, histogram of double spinels divided into groups and stability, relation between mixing enthalpies and cation-oxygen distance, ways of separating double spinels using cation radii. See DOI: 10.1039/x0xx00000x

proposed for Li-based quaternary spinels (37). Together, these results suggest that conventional wisdom regarding the mixing of two spinels is incomplete. Further, such double spinels have a larger cation diversity than the single spinels, which can significantly increase their usability in multiferroic, optoelectronic, superconducting, thermoelectric, and energy storage applications, as well as understanding geochemical and petrological processes. These facts inspire the current work.

In this study we use density functional theory (DFT) to analyze the mixing between normal and inverse spinels over a wide range of chemistries, and explore the possibility of forming an ordered double spinel by calculating their mixing enthalpies. We pair normal and inverse spinels that have one cation in common to form a double spinel, considering three possible cation orderings. From the calculated mixing enthalpies we are able to predict if an ordered double spinel should form, and which cation ordering is more favorable. Initially, we try to understand if the cations prefer one of the two sites in the spinel, and relate the preferred cation site with different cation-specific properties, such as magnetic moment, Bader charge, ionic radius and cation–oxygen distance. To understand the preference for the formation of double spinels, we also study the relation between the change in cation specific properties when a double spinel is formed, and between double spinels with different cation orderings. Additionally, we use the cation-specific properties to sort the double spinels into different spinel types, as well as apply already known methods for sorting single spinels into distinct spinel types depending on the oxidation state of the cation in the tetrahedral site. Finally, we use the Sure Independence Screening and Sparsifying Operator (SISSO) approach (38; 39), which does allow us to classify the double spinels into inverse and normal structures, providing new insight into the driving force for the formation of these spinel structures.

Models and Methodology

The double spinel structure, in this study defined with the chemical formula $ABB'O_4$, is reminiscent of the inverse spinel structure, where two different cations occupy the octahedral sites, while the tetrahedral site is occupied by the third cation. As a model for a double spinel structure we chose the 28-atom structure of $GaAlMgO_4$ generated using cluster expansion (CE) between $(Mg)Al_2O_4$ and $(Ga)MgGaO_4$ normal and inverse spinels, respectively, proposed by Pilania et al. (36). We should point out that there might be other possible arrangements of the cations on the octahedral site as has been shown in some Li-based inverse spinels (37). However, many possible cation orderings were sampled with the CE of $GaAlMgO_4$ and it was found that the current structure has significantly lower energy than any other ordering considered (36). Considering this, and the fact we are screening a large dataset, for the current study we only use the CE-obtained double spinel structure that exhibited a remarkable thermodynamic stability with respect to the two single spinel end points. We considered the mixing between 49 normal and 22 inverse spinels that have been experimentally synthesized (40; 41; 42) and have one common cation, generating 92 double spinel compositions. The list of normal and inverse spinel chemistries considered, along with their calculated total energies, are shown in Table S1. Keeping in mind the different chemistries of the normal, $(A)B_2O_4$, and inverse, $(B')AB'O_4$, spinels, and the two possible sites that the cations can occupy, there

are three fundamental ways the cations can mix in the double spinel structure (assuming a fixed inverse single spinel type ordering on the octahedral sublattice based on Ref. (36)), which we define as:

- DS-Inv₁, with chemical formula $(B')ABO_4$ (inverse spinel)
- DS-Norm, with chemical formula $(A)BB'O_4$ (normal spinel)
- DS-Inv₂, with chemical formula $(B)AB'O_4$ (inverse spinel)

These structural types are illustrated in Fig. 1. The difference between DS-Inv₁ and DS-Inv₂, both of which are inverse structures with a B cation on the tetrahedral sublattice, is which B cation from the two single spinels is on the tetrahedral sublattice. In DS-Inv₁, it is the B' cation from the inverse single spinel, as would be more intuitive. In DS-Inv₂, it is the B cation from the normal spinel, indicating a change in the preferred sublattice for that cation. Ultimately, we tested each of the 92 double spinel compositions in each of the three cation structures to see if they can be formed and determine which of the three cation orderings is the most favourable.

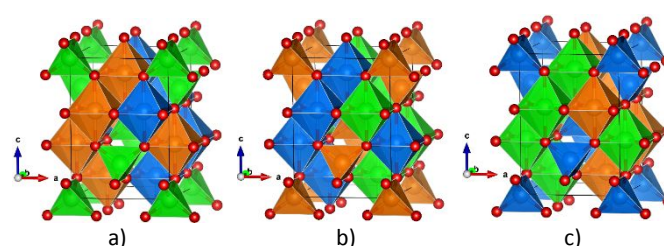


Fig. 1. Ball-and-sticks models of: a) DS-Inv₁ $[(B')ABO_4]$, b) DS-Norm $[(A)BB'O_4]$ and c) DS-Inv₂ $[(B)AB'O_4]$ double spinels. The A, B and B' cations are shown in orange, blue and green, respectively, while the O atoms are in red.

We performed DFT calculations using the Vienna Ab-initio Simulation Package (VASP) code (43; 44; 45; 46), with the generalized gradient approximation of Perdew, Burke and Ernzerhof (PBE) (47) for the exchange-correlation potential, and using the projector augmented wave (PAW) method (48; 49). We used a 520 eV cut-off energy for the plane wave basis set, 10^{-5} eV energy convergence criterion, and $5 \times 5 \times 4$ k -point mesh for both the double and single spinels. All structures were fully relaxed by allowing the volume, cell shape and atomic positions to change during the process. Because of the strongly-correlated nature of the electrons in transition metal oxides, we used the DFT+ U method, with Dudarev's formulation (50): $J = 0$ eV and $U = 5.3, 3.7, 3.9, 5.3, 3.32,$ and 6.2 eV for the systems containing V, Cr, Mn, Fe, Co, and Ni elements, respectively, taken from the Materials Project database (51). In the cases where magnetic elements are present, we considered the following possible magnetic orderings: ferromagnetic and antiferromagnetic in both high and low spin, as well as combinations of ferromagnetic and antiferromagnetic mixing between high and low spin states of the same cation and between different cations. For each of the double spinels we calculated their mixing energy, E_{mix} , using the equation:

$$E_{\text{mix}} = E_{\text{tot}}^{\text{DS}} - \frac{1}{2}(E_{\text{tot}}^{\text{NS}} + E_{\text{tot}}^{\text{IS}}) \quad (1)$$

where $E_{\text{tot}}^{\text{DS}}$, $E_{\text{tot}}^{\text{NS}}$, and $E_{\text{tot}}^{\text{IS}}$ are the total energies per formula unit of the double, normal and inverse spinel, respectively. For each of the single and double spinels in our study we also calculated the Bader charge using the Bader code developed by Henkelman's group (52; 53), using the total charge density. We also performed crystal orbital

Hamiltonian population (COHP) analysis for cation–oxygen and cation–cation interactions as first nearest neighbors of the cations, using the LOBSTER code (54; 55). Additionally, we calculated the integrated COHP (ICOHP) up to the Fermi level, which indicates the bonding strength between the atom pairs.

Results and Discussion

Mixing Enthalpies

In our study we selectively combine 49 normal and 22 inverse spinels with common A cations to form 92 potential double spinels with three different types or cation orderings, and for each of the double spinels we calculated E_{mix} using Eq. (1). Note that E_{mix} is calculated using the lowest calculated energy for each of the two single spinels that are forming the double spinel. We point this out because we reliably reproduce the experimental stability of the single spinels, in terms of whether they are inverse or normal, with the exception of four cases: 1 normal and 3 inverse spinels (see Table S1). The calculated E_{mix} for the 92 double spinels in each of the three cation orderings (types) are summarized in Table S2. Comparing the different types, there are 48, 42 and 2 double spinels having DS-Inv₁, DS-Norm and DS-Inv₂ as the lowest energy ordering, respectively. Further, there are 49 stable double spinels, i.e., double spinels having $E_{\text{mix}} < 0$ eV/formula unit, out of which 30 are DS-Inv₁, 17 are DS-Norm and 2 are DS-Inv₂. These 49 compounds represent 49 potentially new spinels that are yet to be synthesized and might offer new properties and functionality, resulting from their unique chemistries. One should keep in mind that the reported double spinels are thermodynamically stable, which is an important requirement for these compounds to be synthesizable. At finite temperature, the kinetics would have a major influence on the actual synthesis of these double spinels, potentially limiting which structures can be reached in reality, but that is something we cannot probe using our methodology.

We should point out that we also considered a limited number of cases where a reference single spinel might not be the most stable phase at that composition, namely ZnIn₂O₄, GeMg₂O₄, MgTi₂O₄ normal and Zn₂GeO₄, Cd₂GeO₄, Cr₂FeO₄, Fe₂MgO₄ inverse spinels. That is, other crystal structures may be more stable than spinel for these compositions. We found that only two of these other phases are more stable than the respective single spinels, hexagonal Zn₂GeO₄ and Cd₂GeO₄, and we used their total energy to recalculate E_{mix} (see Table S3). Interestingly, in the case of the Zn₂GeO₄, E_{mix} of the double spinel is still < 0 eV/formula unit, even when the new phase is used as a reference, indicating that the hexagonal Zn₂GeO₄ is stabilized in the spinel structure when forming a double spinel. A similar effect has been predicted in perovskites, where specific non-perovskites can be stabilized in a double perovskite structure (56). Note that we only consider stability relative to the starting end-member single spinels, although they might not be the most stable phase for the given composition. This means that there is a possibility for the single spinels to decompose into more stable phases that can thus increase the double spinel mixing energies, eventually making the double spinels unstable.

There are several cases where a given double spinel can be formed from different combinations of reference single spinels. For example, (Co)AlFeO₄ can be made by combining either (Fe)Al₂O₄ and (Co)FeCoO₄ or (Co)Al₂O₄ and (Fe)CoFeO₄. There are five DS-Inv₁ double spinels with $E_{\text{mix}} < 0$ eV in the DS-Inv₁ structure when one combination of single spinels is used as the reference. However,

when a different reference is used, the lowest energy structure becomes DS-Norm with $E_{\text{mix}} > 0$ eV, indicating that these double spinels should decompose to the latter reference single spinels. Note that the labeling of DS-Inv₁ or DS-Norm thus depends on the reference single spinels, while the crystal structure is the same. To understand why these five double spinels are stable when one combination of single spinels is used, and not stable with another, we looked into the composition and relative stability of the reference single spinels. These five double spinels contain Co in tetrahedral positions, in a +2 oxidation state. We compare the relative stability of the single spinels, i.e., is their formation energy on the respective convex hull – see Table S4 with details on the relative stability of the single spinels. In the cases where we predict the DS-Inv₁ double spinel to be stable, both single spinels are less stable than the respective spinels forming the unstable DS-Norm structure. That is, the predicted stability of the DS-Inv₁ structure in these cases is a consequence of the relative instability of the reference single spinel structures. When the lowest energy reference compounds are used, these particular double spinels become unfavorable to form. To understand this difference in stability we focus on the oxidation state of Co in the single spinels. Unlike Fe and Ga that prefer +3 oxidation state, compounds containing Co²⁺ are more stable, one reason being the higher crystal field stabilization energy for Co²⁺. Both of the normal and inverse single spinels that form the DS-Norm have Co in the +2 oxidation state. On the other hand, in the Co₂AO₄ inverse spinel, the Co cations in the tetrahedral and octahedral sites have +2 and +3 oxidation states, respectively, meaning Co is partially in the less favorable +3 oxidation state. This is the main reason why Co₂AO₄ is relatively less stable, making the formation of DS-Inv₁ favorable when those single spinels are used as the reference.

Cation Site Occupancies

The dataset of double spinels that we have is fairly large, and considering the wealth of chemistries that the 17 different cations considered can form, the relation between the stability of the double spinels and cation properties can be very complex. Thus, ideally, we would like to find a simple relation between the properties of the cations and the stability of the double spinels, focusing on the connection between the double spinel mixing energy E_{mix} , the cation type and the different sites it can occupy, see Fig. 2. From Fig. 2 we notice that the distribution of E_{mix} for the cations in DS-Inv₁ and DS-Norm is very similar, while most of the DS-Inv₂ double spinels are unstable, i.e., $E_{\text{mix}} > 0$ eV/formula unit. This is not unexpected because for a DS-Inv₂ structure to form, the B cation from the normal, AB₂O₄, spinel is forced to go from an octahedral into a tetrahedral site, which is not the case for the DS-Inv₁ and DS-Norm double spinels. Considering the small number of stable DS-Inv₂ double spinels, we focus our initial discussion on the DS-Inv₁ and DS-Norm double spinels. Interestingly, Fe, Co and Mn can be found in both tetrahedral and octahedral sites, forming double spinels with E_{mix} distributed around the 0 eV (see Fig. 2). This is expected from the large number of both normal and inverse spinels that these cations can form, occupying both tetrahedral and octahedral site in the single spinels. There are also cations, such as Ga, Ge, Sn, V, Cr Ni, and Rh that form only one type of single spinel, normal or inverse, occupying only one type of site in the stable double spinels, tetrahedral or octahedral. As might be expected, when these cations are in the opposite site than the one in the single spinel, the E_{mix} of the double spinels they form has a large positive value. We also note that looking at the lowest energy type (larger points in Fig. 2) there are several outliers, with $E_{\text{mix}} < -0.5$ eV/formula unit and $E_{\text{mix}} > 0.5$

eV/formula unit. The relation between their stability/instability with the composition and properties will be discussed later.

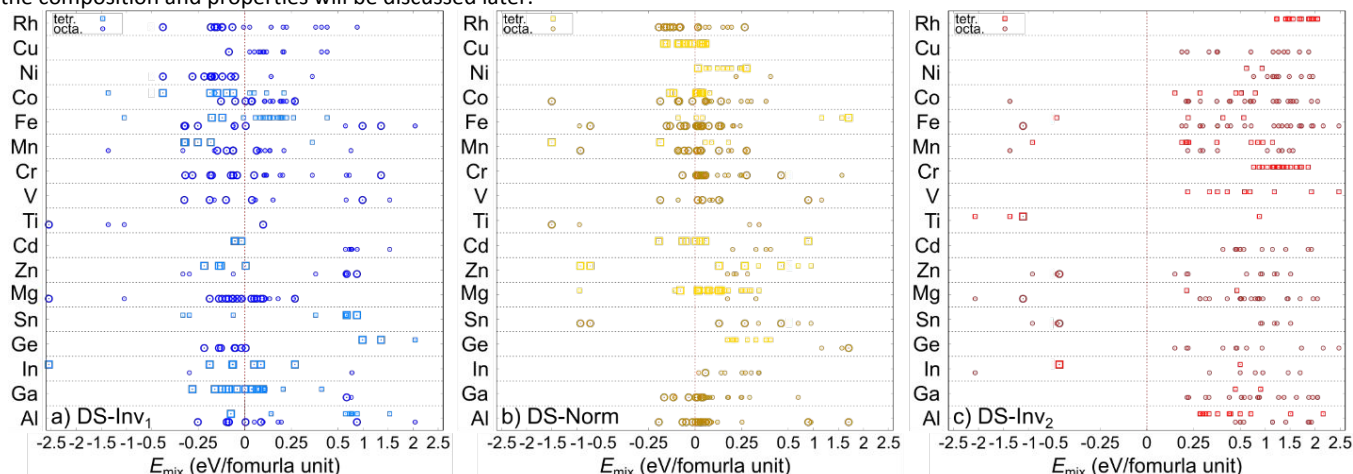


Fig. 2. Relation between the mixing energy (E_{mix}) and the type of cation and site it occupies, for the double spinels with a) DS-Inv₁, b) DS-Norm and c) DS-Inv₂ cation ordering. The tetrahedral and octahedral sites are shown with squares and circles, respectively. The chemistries corresponding to the lowest energy structural types are indicated by larger points

A clearer picture of the preferred cation site in the stable double spinels can be gained by looking at both the lowest energy spinels amongst the three types (the larger points in Fig. 2.) and at the stable double spinels ($E_{\text{mix}} < 0$ eV/formula unit). Figure 3a shows the stable and unstable double spinels per cation site, the cation type and the most stable double spinel type. Cations such as Mg, Cd, Zn, In, Sn, and Ge in tetrahedral site form double spinels where the cation on one of the two octahedral sites is of only one or two chemical species. Also, it is evident that V, Cr, Rh, Ni, Sn and Ge do not form stable spinels when they are located in tetrahedral site. Both of these observations come from the site these cations occupy in the reference single spinels, but does not give us any information regarding how many stable spinels are formed when a cation is located in specific site. Therefore, we plotted the total number and number of stable double spinels per cation, decomposed by the most stable double spinel type and cation site as a histogram, shown in Figure 3b. As mentioned previously, there are a large number of double spinels containing Fe and Co (>30), coming from the large number of single spinels containing these elements and the fact that

these elements can occupy tetrahedral or octahedral site in both normal and inverse spinels. Similarly, Al, Ga, Mg, and Mn also form a relatively large number of double spinels (>20), again a consequence of the significant number of normal and inverse spinels these cations can form. Thus, the predominance of these elements in the double spinels is a reflection of their ubiquity in the single spinels. Looking at the ratio between the stable and total number of spinels (S/T ratio) in Fig. 3b, it is noticeable that the S/T ratio for most of the cations is around $0.5 \pm 1/2$, with few exceptions. Sn and V have very few stable spinels ($S/T < 0.4$), while most of the spinels containing Ti, Ni and Rh are stable ($S/T > 0.7$). Note that the stability of the spinels is not only related to the double spinel energy, it also to the energy of the reference single spinels. Therefore, understanding the preference for forming a large or small number of stable double spinels is related to the double and single spinel chemistry, which is going to be discussed later when the relation between cation properties and E_{mix} is discussed. Going forward, we are going to focus our discussion only on the stable double spinels.

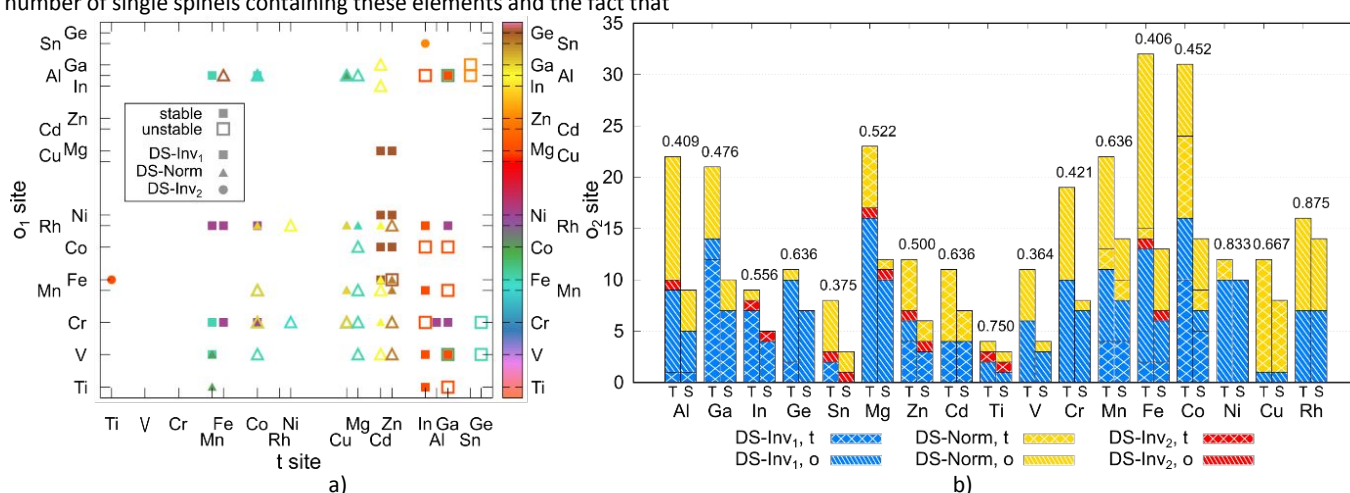


Fig. 3. a) Double spinel stability according to the cation type in tetrahedral (t) and both octahedral (o) sites. The composition of the first octahedral site (o_1) is given on the y axis of the figure while that of the second site (o_2) is given by the color. The stable and unstable spinels are shown with full and open points, respectively. Double spinel cation orderings of DS-Inv₁, DS-Norm and DS-Inv₂ are shown with squares, triangles and circles, respectively. The cation type is ordered according to the Pettifor scale (57). b) Histogram showing the total number (T) and number of stable (S) double spinels per cation, decomposed by the most stable double spinel type and cation site. The most stable DS-

Inv₁, DS-Norm and DS-Inv₁ double spinels are shown in blue, yellow and red, respectively. Whether the cation resides on a tetrahedral (t) and octahedral (o) site in the double spinel structure is shown in lattice and striped pattern, respectively. The number on the top of the bars indicates the ratio between the number of stable and total number of double spinels per cation.

Focusing on the site that the different cations occupy in the stable double spinels, as highlighted in Fig. 3b, it is evident that most of the cations prefer a specific site – either tetrahedral or octahedral – except for Mn, Fe, and Co. This is not unexpected because these three cations can have multiple oxidation states, with different ionic radii and varying crystal field stabilization energies (CFSE), allowing them to accommodate both sites, depending on the other cations present. Consequently, these cations can be found in both tetrahedral and octahedral positions in both types of single spinels as well as in the double spinels. Additionally, V³⁺, Rh³⁺, Cr³⁺, Ti⁴⁺/Ti²⁺ and Ni²⁺ have a high CFSE and thus have a strong octahedral site preference. Cations with shallow valence d-states, such as Zn²⁺, Cd²⁺, In³⁺, and Ga³⁺, prefer the tetrahedral site. Mg²⁺, Al³⁺ and Ge⁴⁺ have octahedral site preference (OSP), a quantity indicating the preference for the ion to occupy the octahedral site, derived from the degree of inversion of single spinels and their experimentally measured formation enthalpies (58; 59). The only disagreement in our calculations with the OSP model is for the Cu²⁺ cation, for which the model predicts a moderate OSP but we find a preference for the tetrahedral site. One reason for this can be the presence of cations with higher OSP than Cu²⁺. However, although in the Cu²⁺ containing double spinels one octahedral site is occupied by Mn³⁺, Rh³⁺, Cr³⁺, and Al³⁺ cations, the other site is always occupied by Ga³⁺, Fe³⁺ and Co³⁺ cations, all of which have smaller predicted OSP than Cu²⁺. Hence, the almost-filled d-orbitals in Cu²⁺ possibly dominate in the bonding, forcing Cu²⁺ in the tetrahedral site. This suggests that a further analysis of single spinels containing Cu²⁺ and varying chemistries could be used to improve the experimental OSP models.

Additionally, there are five exceptions in which cations do not reside on the expected sites: one case each of Al³⁺, Mg²⁺ and Ti⁴⁺ on the tetrahedral site, and one case each of Zn²⁺ and Cu²⁺ on the octahedral site. To understand why these cations do not occupy their nominally preferred site, we looked into the composition of the associated double spinels, specifically the cations that compete for their preferred site. In the case of Al³⁺ and Mg²⁺, the double spinels are (Al)NiCrO₄ and (Mg)RhFeO₄, where both Al³⁺ and Mg²⁺ are competing with transition metal ions for the octahedral site, Ni²⁺/Cr³⁺ and Fe³⁺/Rh³⁺, respectively. Because of CFSE, the transition metals have higher OSP compared to Al³⁺ and Mg²⁺, and thus preferably occupy the octahedral site. In the double spinels (Ga)CuAlO₄ and (In)SnZnO₄, Cu²⁺ and Zn²⁺ are competing with Ga³⁺ and In³⁺ for the tetrahedral site, respectively, and ultimately the larger ions with higher charge have a stronger preference for the tetrahedral site. In the (Ti)FeMgO₄ spinel Ti is in a +4 oxidation state, and hence its OSP due to CFSE is 0, while Fe²⁺ has a preference for octahedral site and its CFSE is 0.133 eV. Although Reznitskii (60) predicts higher OSP for Ti⁴⁺ than Mg²⁺, our results show that the cation with higher charge, Ti⁴⁺, would preferably occupy the tetrahedral site.

Interestingly, two of the exceptional cases, (In)SnZnO₄ and (Ti)FeMgO₄, are the only two cases in which the double spinel adopts the DS-Inv₂ type cation ordering, indicating that one of the driving forces for forming such a structure is allowing one of the cations to reside in its preferred site when it was forced to adopt the less preferred site in the single spinel, e.g. Mg in tetrahedral site in (Ti)FeMgO₄, and In in octahedral site (In)SnZnO₄. Note that, in addition to the factors discussed in the preceding paragraphs, other factors also contribute to the stability of the double spinels, such as the relative stability of the reference single spinel, which are discussed below in Sec 3.3 for the (Ti)FeMgO₄ case.

Previously we showed that with exception of Mn, Fe and Co, all other cations have a preferred site, tetrahedral or octahedral. Here, we aim to understand whether there is any relation between the stability of the double spinels and cation-specific properties; specifically, we consider Bader charge (q_{bader}), magnetic moment (μ), and cation–oxygen distance ($d_{\text{M-O}}$). In particular, we are interested in the change in these properties between the double spinel and the associated reference single spinels (Δq_{bader} , $\Delta\mu$ and $\Delta d_{\text{M-O}}$), providing information on what might be the driving force behind the formation of stable double spinels. Figure 4 shows the distribution of Δq_{bader} , $\Delta\mu$ and $\Delta d_{\text{M-O}}$ as violin plots, depending on the cation site, both for all double spinel structures considered (left of each plot) and only for the stable double spinels ($\Delta E_{\text{mix}} < 0$ eV/formula unit; right of each plot). Note that for clarity we show the distribution of Δq_{bader} , $\Delta\mu$ and $\Delta d_{\text{M-O}}$ for four cations, while the violin plots for every cation are shown in Fig. S1. For Δq_{bader} and $\Delta\mu$ we chose only transition metals to highlight the relation between the oxidation state (Δq_{bader}) and magnetic moment ($\Delta\mu$), while, for the purpose of higher diversity of chemistry, for $\Delta d_{\text{M-O}}$ we chose two main group cations and two transition metals. Interestingly, $\Delta d_{\text{M-O}}$ in the stable double spinels has a narrower distribution around 0 Å compared to the total number of double spinels, shown by the box-plots in Fig. 4. This indicates that in stable compounds the cations prefer having the same distance to the oxygen atoms in the double spinel structures as they have in the single spinels, minimizing strain. Δq_{bader} and $\Delta\mu$ exhibit similar behavior to each other, a consequence of their common relation to the cation oxidation state. Co is the only exception, which can be seen switching between high and low spin states without correspondingly large changes in Δq_{bader} . Because of the magnetic behavior of Co, and the relation between Δq_{bader} and $\Delta\mu$, we do not show the box plots for $\Delta\mu$. Similarly to $\Delta d_{\text{M-O}}$, Δq_{bader} has a somewhat narrower distribution for the stable double spinels than the total number of spinels (compare box plots in Fig. 4), but this distribution is broader than that of $\Delta d_{\text{M-O}}$. The broader distribution of Δq_{bader} comes from a few outliers, where $\Delta q_{\text{bader}} < -0.5 e$ or $\Delta q_{\text{bader}} > 0.5 e$, indicating that there are a few cases where the cation oxidation state present in the single spinel changes when the double spinel is formed.

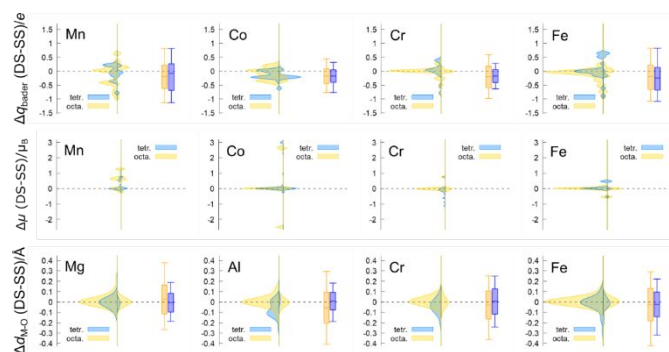


Fig. 4. Violin plots showing the distribution of changes in the Bader charge (Δq_{bader} , top), magnetic moment ($\Delta\mu$, middle), and cation–oxygen distance ($\Delta d_{\text{M-O}}$, bottom) in the double spinel (DS) and the reference single spinels (SS) for four different cations. The cation site (tetrahedral and octahedral) is indicated in blue and yellow, respectively. The distribution for each property in all spinel structures considered vs only in the stable double spinels is shown in the left and right part of each violin plot, respectively. The box-plots

for the total number and stable double spinels are shown in orange and purple, respectively.

Understanding Stability

Let us now return to the outliers in Fig. 2. There are 4 double spinels with $E_{\text{mix}} < -0.5$ eV/formula unit, containing 8 different cations, and 6 double spinels with $E_{\text{mix}} > 0.5$ eV/formula unit, containing 9 different cations. These 10 double spinels are listed in Table 1, together with their reference single spinels, E_{mix} and the lowest energy double spinel type. Initially, we will focus on the stable double spinels, specifically (Ti)CoMnO₄, (Ti)MgFeO₄, and (Zn)MnSnO₄. In each of these double spinels, Ti and Sn are in their most stable +4 oxidation state, as compared to the +3 and +2/+4 oxidation states they exhibit in the single spinels, respectively. The other cations either have a strictly +2 oxidation state (Mg and Zn), or can easily form spinels with both +2 and +3 oxidation states: Fe, Mn and Co. Hence, the biggest driving force for stability of these double spinels is the formation of the favorable +4 oxidation state of the Ti and Sn cations, from their frustrated +3 and +2 oxidation states in the single spinels. (In)MgTiO₄ is slightly different, in the sense that none of the cations changes oxidation state from the reference single spinels when forming the double spinel. Thus, the stability of this double spinel can come from either the relatively unstable reference single spinels or the favorable chemistry in the double spinel. Interestingly, each cation in this double spinel is in its preferred site, i.e., In in the tetrahedral and Ti/Mg in the octahedral site (see Fig. 3). On the other hand, in both single spinel references, one cation is in the less preferred site, Mg in the tetrahedral site in the normal spinel, and In in the octahedral site in the inverse spinel. This means that any frustration in the structure because of the occupation of a non-preferred site is completely removed when the double spinel is formed, which can explain the significant driving force to form the (In)MgTiO₄ double spinel.

Table 1. List of double spinels with $E_{\text{mix}} < -0.5$ eV/formula unit or $E_{\text{mix}} > 0.5$ eV/formula unit (outliers in Fig. 2), with the reference single spinels, and the E_{mix} of the most stable type.

Normal spinel	Inverse spinel	Double spinel	Type	E_{mix} (eV/fu)	Spinel group
MgTi ₂ O ₄	In ₂ MgO ₄	(In)MgTiO ₄	DS-Inv ₁	-2.5479	2-3 Inverse
MnTi ₂ O ₄	Co ₂ MnO ₄	(Mn)TiCoO ₄	DS-Norm	-1.4981	2-4 Inverse
MgTi ₂ O ₄	Fe ₂ MgO ₄	(Ti)MgFeO ₄	DS-Inv ₂	-1.1102	2-4 Normal
ZnMn ₂ O ₄	Sn ₂ ZnO ₄	(Zn)MnSnO ₄	DS-Norm	-0.9257	2-4 Inverse
ZnFe ₂ O ₄	Sn ₂ ZnO ₄	(Zn)FeSnO ₄	DS-Norm	-0.7303	2-4 Inverse
ZnGa ₂ O ₄	Sn ₂ ZnO ₄	(Sn)GaZnO ₄	DS-Inv ₁	0.6737	2-3 Inverse
ZnAl ₂ O ₄	Sn ₂ ZnO ₄	(Sn)AlZnO ₄	DS-Inv ₁	0.8791	2-3 Inverse
CdV ₂ O ₄	Al ₂ CdO ₄	(Cd)AlVO ₄	DS-Norm	0.9003	2-3 Normal
FeV ₂ O ₄	Ge ₂ FeO ₄	(Ge)FeVO ₄	DS-Inv ₁	0.9904	2-3 Inverse
FeCr ₂ O ₄	Ge ₂ FeO ₄	(Ge)FeCrO ₄	DS-Inv ₁	1.3604	2-3 Inverse
FeAl ₂ O ₄	Ge ₂ FeO ₄	(Fe)AlGeO ₄	DS-Norm	1.7070	2-3 Normal

We now consider the unstable spinels. In the case of the Ge-containing unstable spinels, it is evident that Ge comes from Ge₂FeO₄ inverse spinel, where Ge is in both +2 and +4 oxidation states, and Fe is in +2 oxidation state. However, unlike the inverse single spinel, the third cation in the Ge double spinels is in +3 oxidation state, forcing the formation of Fe³⁺, leaving all of the Ge to take on the unfavorable +2 oxidation state. Similarly, in the Sn containing unstable double spinels, Sn is forced into a highly unfavorable +3 oxidation state by the +3 oxidation state of the third cation. This can explain why these Ge and Sn containing double spinels are very unstable. The (Cd)AlVO₄ double spinel is slightly different because the cations are in their favorable oxidation states, +2, +3 and +3 for Cd, Al and V,

respectively, and they are all in their preferred site: Cd in the tetrahedral and Al/V in the octahedral site. Thus, to understand where the instability for this compound comes from, we need to look into the relative stability of the reference single spinels, as well as the change in cation properties when forming the double spinel. We compared cation-specific properties, such as Bader charge, magnetic moment, cation–oxygen distance, ionic radius and ICOHP, in the double spinel and the reference single spinels. The only noticeable difference is in the ICOHP, where the most significant change is in the Al–O and V–O bonding strength, with the ICOHP difference between the double and single spinel being -0.56 and 1.20 per formula unit, respectively. Although the Al–O bond strength is increased in the double spinel, the V–O bond strength is decreased to an even greater extent, destabilizing the structure, increasing its energy, and thus making (Cd)AlVO₄ less stable. The decrease in V–O bond strength in the double spinel might be related to the high stability of the (Cd)V₂O₄ single spinel used to make the double spinel. Notably, it seems that all (M)V₂O₄ normal spinels are very stable, giving rise to a small amount of V containing double spinels, having a 0.364 S/T ratio.

We just showed that, in both the most stable ($E_{\text{mix}} < -0.5$ eV) and the most unstable ($E_{\text{mix}} > 0.5$ eV) double spinels, the oxidation state of the cations tends to become more favorable or less favorable, respectively. Interestingly, this change in oxidation state in the stable double spinels is reflected in the few outliers in Δq_{bader} , as previously discussed (Fig. 4 and Fig. S1). However, the change in oxidation state cannot explain the stability for most of the stable double spinels, which entails a further analysis of the change in cation-specific properties between the double spinels and reference single spinels. Because both the Bader charge and magnetic moment are related to the cation oxidation state, we focus only on the $d_{\text{M-O}}$ distance, the cationic radius (r_i), and the band gap (E_g) in our analysis. We emphasize the difference in the properties between the double spinel and reference single spinels, as a function of E_{mix} , as well as the difference in the properties between DS-Inv₁ and DS-Norm double spinels, the most common structures found in our set. Furthermore, following the notation used for single spinels, we divided the studied double spinels into two groups: 2-3 and 4-2 spinels, with normal and inverse ordering, depending on the oxidation state of the cations in the octahedral site. For example, if both cations in the octahedral site are in +3 oxidation state, then that spinel is 2-3 normal, while if both cations are in +2 oxidation state, then the spinel is 4-2 normal. Shown in Fig. S2 is the number of double spinels with DS-Inv₁ and DS-Norm ordering, divided into the 4 spinel groups (2-3 and 4-2 spinels, each having normal and inverse ordering), separately considering the total number and number of stable double spinels.

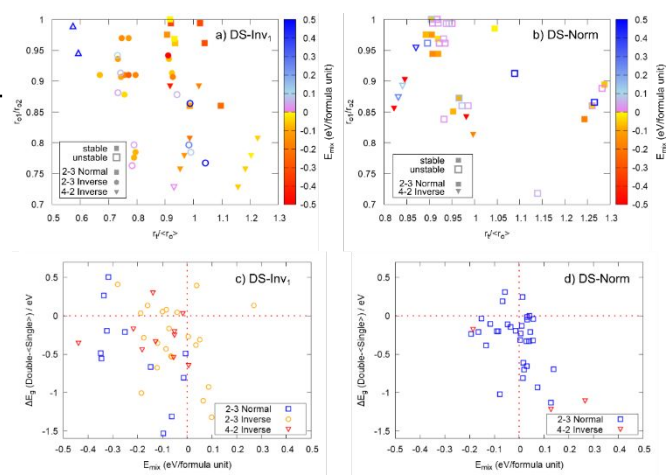


Fig. 5. (top) Relation between the ratio of the tetrahedral (r_t)/average octahedral ($\langle r_o \rangle$) ionic radii and the ratio of the cation radii of the two octahedral sites in: a) DS-Inv₁ and b) DS-Norm double spinels. Filled and open points show stable and unstable double spinels, respectively. (bottom) Difference between the band gap (E_g) in double spinels (Double) and the average band gap of the reference single spinels ($\langle \text{Single} \rangle$) as a function of the mixing energy (E_{mix}) in: c) DS-Inv₁ d) DS-2nd d) DS-Norm double spinels. The 2-3 normal, 2-3 inverse and 4-2 inverse spinel groups are shown with squares, circles and triangles, respectively.

In the case of d_{M-O} , we do not find any clear relation between the difference in d_{M-O} in the double spinels and reference single spinels as a function of E_{mix} (Fig. S3a and b). Comparing d_{M-O} between the two different double spinel types, we do see that there is a clear separation between d_{M-O} in the tetrahedral and octahedral site (Fig. S3c), but this is expected because of the different coordination at the sites. In the case of r_i , we looked at the relationship between E_{mix} and both the difference (Fig. S4a and b) and ratio (Fig. 5a and b) between r_i of the tetrahedral and octahedral site, as well as their absolute values. We find a clustering of stable and unstable DS-Inv₁ and DS-Norm double spinels, respectively, in the top center of the r_i ratio plots (Figs. 5a and b). However, there is no clear separation of the stable and unstable double spinels of different types depending on the r_i ratios. We also looked at the difference in E_g between the double spinels and reference single spinels ($E_g(\text{Double}-\langle \text{Single} \rangle)$) as a function of E_{mix} for the different double spinel types and spinel groups. A rough linear trend between $E_g(\text{Double}-\langle \text{Single} \rangle)$ and E_{mix} can be observed (Fig. 5c and d), with a negative slope, meaning that with decreasing E_{mix} the double spinel band gap with respect to the single spinel is increasing. This relation is not unexpected, coming from the general rule that an increasing bandgap would stabilize a compound; however the relation is poor as indicated by the largely scattered points. Also, we checked if an increasing charge on the oxygen atom, consequently decreasing the charge on the cations and increasing the bond strength (following a simple Coulombic attraction), has any influence on the stability of the double spinels, but this did not give any meaningful correlation. Additionally, we applied methods used for separating single spinels into different groups based on the anionic parameter u , namely the methods suggested by Sickafus et. al. (61), Yokoyama et. al. (62) and Stevanović et. al. (42), shown Fig. S5. Unfortunately, none of these methods could successfully separate the double spinel types into their respective types or spinel group.

Classifying Double Spinels with Machine Learning

Clearly, our analysis shows that there is no single elemental property of either the cations within the spinels or the spinels themselves that provide any predictive capability to classify the double spinels into their respective structural types. Thus, we focus on understanding physical factors that dictate whether a double spinel chemistry formed by combining two single spinels is likely to adopt a DS-Inv₁ or DS-Norm double spinel configuration. We start by exploring simple correlations between various elementary features of the different elements forming the double spinels with the DFT calculated absolute and relative stabilities of DS-Inv₁ or DS-Norm double spinels. Our exploratory analysis provided strong indications that local-coordination-environment-dependent relative size effects of different cations going from single to double spinels play an important role in the stabilization of either DS-Inv₁ or DS-Norm double spinels. To illustrate a concrete example, in Fig. 6(a) we plot the absolute difference of Shannon's ionic radii for tetrahedrally-

coordinated A and B' cations in a given double spinel against the DFT-calculated DS-Inv₁ double spinel mixing enthalpies (E_{mix}) over the entire double spinel dataset. The rationale behind choosing the specific cation radii stems from the fact that while A cations occupy the tetrahedral sites in a normal spinel, in a DS-Inv₁ double spinel all of the IV-fold coordinated sites are occupied by the B' cations. Therefore, if Shannon's ionic radii for the A and B' cations differ significantly, one would expect that the resulting double spinel chemistry would be destabilized due to unfavorable local strain effects. Indeed, from Fig. 6(a) it can be seen that most stable DS-Inv₁ double spinels exhibit a relatively small value of $|R(A_T)-R(B'_T)|$, whereas for the unstable DS-Inv₁ double spinel chemistries (i.e., $E_{\text{mix}} > 0$), a rough linear trend of E_{mix} with the $|R(A_T)-R(B'_T)|$ is seen. Although such qualitative notions indicate the importance of the local strain effects at the tetrahedral sublattice in the stabilization of a particular double spinel, the observed rough correlations further point to the possibility that effects related to local strain on the octahedral sublattice and/or factors other than the local strain effects might also be important.

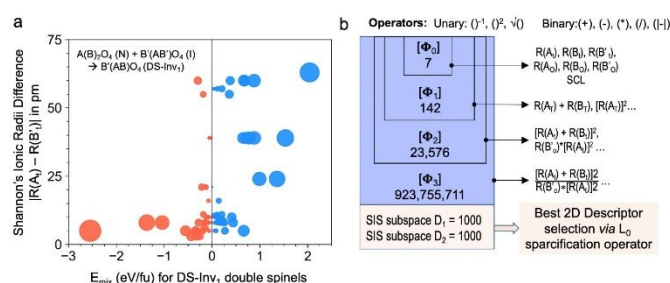


Fig. 6. (a) Variation of the absolute difference of Shannon's ionic radii for tetrahedrally-coordinated double spinel A and B' cations with the DS-Inv₁ double spinel mixing enthalpies (E_{mix}). The red and blue circles show chemistries with negative and positive E_{mix} , respectively, and the size of the symbols indicates the magnitude of E_{mix} . (b) Schematic representation of iterative feature set accumulation via combining a set of primary features in Φ_0 with the selected set of unary and binary operators shown on the top. This large feature space was subsequently used to identify the best 2D descriptor separating chemistries with the DS-Inv₁ and DS-Norm structures as their ground states via application of the SISO approach (see text for details).

To systematically explore these factors and to identify a simple and physically-intuitive descriptor for classifying the double spinels, we employ the SISO approach (38; 39) based on the compressed sensing technique. This approach allows for efficient exploration of vast descriptor spaces (with the number of unique descriptors typically reaching up to several billions) and has recently been applied to a number of materials design and discovery problems (63; 64; 65; 66). To generate a classification model for predicting the relative stability of a double spinel chemistry in the DS-Inv₁ versus DS-Norm structure, we start with a set of six Shannon ionic radii and one categorical variable defined for the DS-Norm double spinels (referred to as the spinel classification label SCL) as primary descriptors. We consider both the tetrahedral- and octahedral-coordinated ionic radii for each of the three cations, namely, $R(A_T)$, $R(B_T)$, $R(B'_T)$ and $R(A_O)$, $R(B_O)$, $R(B'_O)$. SCL not only labels the 2-3 and 4-2 type of cation charge states for the double spinels but also distinguishes whether the cations on the octahedral sublattice exhibit a uniform nominal oxidation state or not. More specifically, SCL adopts negative and positive integer values for the DS-Norm

ARTICLE

double spinels with 2-3 and 4-2 type of cation oxidation states, respectively, and we use $|SCL| = 1$ or 2 depending on whether the cations on the octahedral sublattice show a one or two different oxidation states. We note that the specific choice of the categorical label was based on past studies on 2-3 and 4-2 group single spinels where the two classes are known to show qualitatively different trends in local electrostatic interactions (40). Moreover, past classification models targeted towards separating normal and inverse spinels have benefited from incorporation of a categorical variable that explicitly distinguishes the 2-3 and 4-2 type of cation oxidation states for single spinels (42).

Starting with the primary features (feature space Φ_0 in Fig. 6(b)), the SISSO method enumerates a large set of features by iteratively applying a set of prespecified algebraic operations on the current feature space. This iterative procedure leads to a truly vast set of descriptors of increasing complexity *via* combinatorial explosion. As illustrated in Fig. 6(b), combining the seven primary features outlined above with three unary operators ($^{-1}$, 2 , $\sqrt{\quad}$) and five binary operators ($+$, $-$, $*$, $/$ and $|-|$) leads to 142, 23,576 and 923,755,711 descriptors in the first, second and third generations, giving rise to nearly a billion total descriptors in the combined feature space $\Phi_0 \cup \Phi_1 \cup \Phi_2 \cup \Phi_3$. We also note here that, to focus on physically relevant descriptors, the SISSO approach explicitly accounts for the feature units and only features with the same units are combined using the binary operators. As a next step, to identify the best set of descriptors for the classification problem at hand, the SISSO method employs the sure-independence screening (SIS) method and the sparse solution algorithm using sparsifying operators (SO) in synergy. Starting with the accumulated set of feature space, the SIS method selects a subspace of features with the best classification performance quantified via targeting for an overlap region with the least number of samples and a minimum area. The SO step then evaluates all possible combinations of features from the SIS subspace, yielding the optimal solution. In the present case, a SIS subspace of 1000 was consistently used for identifying the optimal 1D descriptor and the 2D descriptor pair, henceforth referred to as (D_1, D_2) . Further details of the SISSO method can be found in Refs. (38; 39).

The classification achieved with the best descriptor pair identified via the SISSO approach is presented in Fig. 7(a). The inset depicts a magnified view of a very small overlap region formed by the convex hulls for the two double spinel types, namely DS-Inv₁ and DS-Norm, identified with the blue and red markers, respectively. Further, the area of the circular markers in the figure represents the absolute value of the relative mixing enthalpies between the two double spinel types (i.e., $|\Delta E_{\text{mix}}| = |E_{\text{mix}}(\text{DS-Inv}_1) - E_{\text{mix}}(\text{DS-Norm})|$) and therefore provides a graphical depiction of their relative stabilities. While the identified optimal 2D descriptor does not lead to a perfect classification, it can be seen from the inset in Fig. 7(a) that all of the double spinels falling within the overlap region consistently exhibit a much lower value of $|\Delta E_{\text{mix}}|$ -- that is, they are on the cusp of stability between the two structural types.

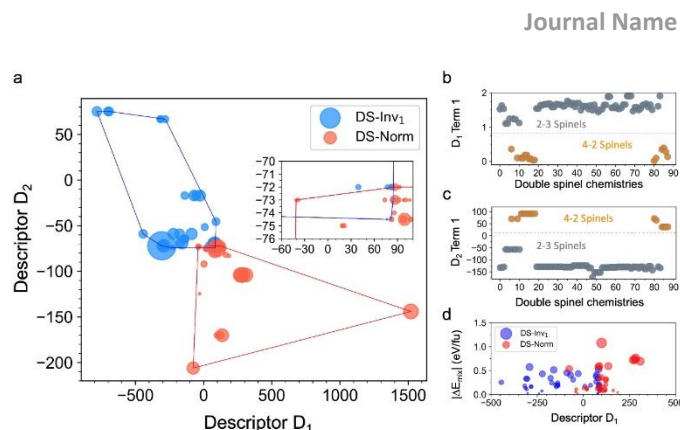


Fig. 7. (a) Performance of the SISSO-identified best 2D descriptor (D_1, D_2) in classifying the DS-Inv₁ and DS-Norm double spinel configurations. The red and blue circles show chemistries with DS-Norm and DS-Inv₁ ground states, respectively, and the size of the symbols indicates the magnitude of the relative difference between the energetics of the two structures for a given chemistry. The inset shown an enlarged view of the overlap region formed by the two convex hulls encompassing the DS-Inv₁ and DS-Norm stability regions in the structure map. (b) and (c) show the role of a specific term in descriptors D_1 and D_2 , respectively. (d) Classification performance obtained by using just the first descriptor D_1 of the optimal 2D descriptor. The plotting scheme in (d) is same as that of (a).

To gain deeper insight into the classification performance, next we take a closer look at the various component terms constituting the identified descriptor pair (D_1, D_2) , where,

$$D_1 = \left[\frac{R(B_t)}{R(A_o)} - \frac{1}{SCL} \right] * \left[(R(A_o) - R(B'_o)) * |R(A_t) - R(B'_o)| \right] \quad (2)$$

$$D_2 = \frac{R(A_o) + R(A_t)}{SCL} - [SCL * R(B'_o) + |R(A_t) - R(B'_o)|] \quad (3)$$

The second terms, identified in square brackets in Eqs. 2 and 3, for both descriptors D_1 and D_2 can be visually recognized to be largely dominated by size effects—the original premise that motivated the descriptor analysis. It is also interesting to note that these terms share a common expression $|R(A_t) - R(B'_o)|$, which essentially captures relative local strain effects caused by forming a double spinel by combining two single spinels, one normal and another inverse. More precisely, note that going from normal $(A)B_2O_4$ and inverse $(B')AB'O_4$ single spinels to a DS-Inv₁ (inverse) double spinel $(B')ABO_4$ both the A (fully) and B' (partially) cations swap their coordination environments and therefore it is intuitively expected that the relative trends in their coordination-dependent ionic radii across the chemistry would contribute towards their energetic stabilization in a particular double spinel structure. A similar, or perhaps stronger, argument can also be made for cations in a single inverse spinel $(B')AB'O_4$ that participate to form a DS-Norm (normal) double spinel $(A)BB'O_4$. While the second terms in each of the two expressions can straightforwardly be traced to the local strain effects, the role of the first terms is a bit more difficult to comprehend by a visual inspection alone. Plotting each of these two terms in Figs. 7(b, c), however, readily reveals that both terms essentially play an identical role in the construction of the two descriptors, viz., separating the double spinel chemistries based on their cation electrostatics, i.e., spinels formed by 2-3 versus 4-2 cation oxidation states. Naturally, the categorical feature SCL plays a dominant role in these terms. Subsequently, via combining the first electrostatics-dominated term with the second local strain-

dominated term, for instance in D_1 as shown in Fig. 7(d), enables us to classify DS-Inv₁ versus DS-Norm double spinels, albeit with a relatively larger overlap region which shrinks dramatically going to a 2D descriptor [cf. Fig. 7(a)].

Summary of Primary Results and Implications

Our DFT calculations have shown that, by mixing various single spinel calculations, a number of new thermodynamically stable compounds that we have termed double spinels exist. Our primary results include:

- 49 stable double spinels are predicted to have a thermodynamic tendency to form from normal (A)[B₂]O₄ and inverse (B')[AB']O₄ spinels that have one common cation, primarily having one of two cation orderings: (B')[AB]O₄ and (A)[BB']O₄.
- Identifying the possibility of stabilizing non-spinel structures in a double spinel configuration, for cases where the non-spinel structure has lower energy compared to the single spinel with same composition.
- Of the three cations comprising the double spinels, each typically occupies a specific site, octahedral or tetrahedral, which might be different from that occupied in the reference single spinels. The only exceptions are Mn, Fe and Co that can occupy either of the two sites.
- Using only cation specific properties, we used machine learning to successfully classify the double spinels via their cation orderings, showing that interplay of both strain and electrostatics drives the difference between the cation orderings and whether the double spinel is inverse or normal in nature.

The discovery and identification of these novel compounds provide a unique opportunity for designing materials with new functionalities. Similar to the promise offered by double perovskites, the predicted existence of double spinels grants an additional set of chemistries for this versatile crystal structure that could present new properties for a range of applications. Specifically, the inclusion of three cations, and their associated variety, into an ordered spinel structure greatly expands the spinel design space, increasing the potential applications of these compounds: for thermoelectric applications where the lattice thermal conductivity can be reduced because of cations with different mass; as cathode materials in high-voltage batteries by utilizing the transport of +2 and +3 cations; for optical applications where the variable composition aids in tailoring the band gaps of the double spinels to specific needs; for spin filtering applications where half-metallic properties are needed; or multiferroic properties that can be generated from the multiple magnetic elements in the double spinels.

Conclusions

Using high-throughput first-principles calculations, we screened a list of 92 double spinel chemistries with three different cation orderings for their stability with respect to reference normal (A)B₂O₄ and inverse (B')AB'O₄ spinels. We found 49 stable double spinels, primarily having (B')ABO₄ (DS-Inv₁) and (A)BB'O₄ (DS-Norm) ordering of the cations. Looking at the site that different cations occupy in the stable spinels, we find a clear preference for the tetrahedral or octahedral site depending on the nature of the cation, with Fe, Mn and Co being the only exceptions. We argue that the different behavior of Fe, Mn and

Co comes from their varying oxidation states in the double spinels, and the octahedral site stabilization energy related to the different oxidation states. We show that the differences in Bader charge and cation–oxygen distance between the double spinels and their reference single spinels is smaller in the stable spinels compared to the whole list of potential double spinel compounds. Still, we show that the most stable double spinels, with $E_{\text{mix}} < -0.5$ eV/formula unit, are stabilized by a change in oxidation state of one of the cations. However, we were not able to find any meaningful relation between E_{mix} and cation-specific properties, nor with the difference in properties between the double spinel with different cation orderings. Additionally, we show that strain on the tetrahedral site influences the stability of the double spinels. Finally, we were able to successfully classify the double spinel chemistries into different double spinel structures using complex descriptors produced by SISSO. A careful examination of the form of the two descriptors showed that the ability of these two descriptors to classify the double spinel compounds between the different double spinel cation structural types comes from both strain and electrostatic dominated terms.

Conflicts of interest

The authors declare that they have no competing interests.

Acknowledgements

This work, performed at Los Alamos National Laboratory, was supported by the U.S. Department of Energy, Office of Science, Basic Energy Sciences, Materials Sciences and Engineering Division. Los Alamos National Laboratory is operated by Triad National Security, LLC, for the National Nuclear Security Administration of U.S. Department of Energy (Contract No. 89233218CNA000001). Computational support for this work was provided by LANL's high performance computing clusters.

References

1. *Spinel as petrogenetic indicators: Activity-composition relations at low pressures.* Sack, Richard O. s.l. : Springer Science and Business Media LLC, 1982, Contributions to Mineralogy and Petrology, Vol. 79, pp. 169–186.
2. *Spinel-Layered Core-Shell Cathode Materials for Li-Ion Batteries.* Cho, Yonghyun, et al. s.l. : Wiley, 7 2011, Advanced Energy Materials, Vol. 1, pp. 821–828.
3. *Investigation of structural, elastic, electronic, optical and vibrational properties of silver chromate spinels: Normal (CrAg2O4) and inverse (Ag2CrO4).* Kushwaha, A. K., et al. s.l. : Elsevier BV, 5 2017, Journal of Alloys and Compounds, Vol. 704, pp. 101–108.
4. *Microwave applications of soft ferrites.* Pardavi-Horvath, Martha. s.l. : Elsevier BV, 6 2000, Journal of Magnetism and Magnetic Materials, Vols. 215-216, pp. 171–183.

5. *Electrochemical Luminescence of Rare Earth Metal Ion Doped MgIn₂O₄ Electrodes*. **Sonoyama, Noriyuki, et al.** s.l. : The Electrochemical Society, 2006, Journal of The Electrochemical Society, Vol. 153, p. H45.
6. *Preparation of LiTi₂O₄ single crystals with the spinel structure*. **Akimoto, J., et al.** s.l. : Elsevier BV, 2 1992, Journal of Solid State Chemistry, Vol. 96, pp. 446–450.
7. *Superconducting and normal state properties of Li_{1-x}Ti_{2-x}O₄ spinel compounds. {II}. Low-temperature heat capacity*. **McCallum, R. W., et al.** s.l. : Springer Science and Business Media LLC, 10 1976, Journal of Low Temperature Physics, Vol. 25, pp. 177–193.
8. *Nanostructured ferrites: Structural analysis and catalytic activity*. **Albuquerque, Adriana S., et al.** s.l. : Elsevier BV, 4 2012, Ceramics International, Vol. 38, pp. 2225–2231.
9. *Spinel ferrites as catalysts: A study on catalytic effect of coprecipitated ferrites on hydrogen peroxide decomposition*. **Lahiri, Preeti and Sengupta, Susanta K.** s.l. : Canadian Science Publishing, 1 1991, Canadian Journal of Chemistry, Vol. 69, pp. 33–36.
10. *Research Update: Photoelectrochemical water splitting and photocatalytic hydrogen production using ferrites (MFe₂O₄) under visible light irradiation*. **Dillert, Ralf, et al.** s.l. : AIP Publishing, 10 2015, APL Materials, Vol. 3, p. 104001.
11. *Co₃O₄ nanocrystals on graphene as a synergistic catalyst for oxygen reduction reaction*. **Liang, Yongye, et al.** s.l. : Springer Science and Business Media LLC, 8 2011, Nature Materials, Vol. 10, pp. 780–786.
12. *Thermodynamic Stability, Redox Properties, and Reactivity of Mn₃O₄, Fe₃O₄, and Co₃O₄ Model Catalysts for N₂O Decomposition: Resolving the Origins of Steady Turnover*. **Kaczmarczyk, Jan, et al.** s.l. : American Chemical Society (ACS), 1 2016, ACS Catalysis, Vol. 6, pp. 1235–1246.
13. *The spinels: versatile materials*. **Grimes, N. W.** s.l. : IOP Publishing, 1 1975, Physics in Technology, Vol. 6, pp. 22–27.
14. *Magnetic Reversal of the Ferroelectric Polarization in a Multiferroic Spinel Oxide*. **Yamasaki, Y., et al.** s.l. : American Physical Society (APS), 5 2006, Physical Review Letters, Vol. 96.
15. *An overview of the structure and magnetism of spinel ferrite nanoparticles and their synthesis in microemulsions*. **Mathew, Daliya S. and Juang, Ruey-Shin.** s.l. : Elsevier BV, 5 2007, Chemical Engineering Journal, Vol. 129, pp. 51–65.
16. *Magnetism, microstructure and crystal chemistry of spinel ferrites*. **van Groenou, A. Broese, Bongers, P. F. and Stuyts, A. L.** s.l. : Elsevier BV, 2 1969, Materials Science and Engineering, Vol. 3, pp. 317–392.
17. *Insulating Ferromagnetic Spinel*. **Baltzer, P. K., Lehmann, H. W. and Robbins, M.** s.l. : American Physical Society (APS), 9 1965, Physical Review Letters, Vol. 15, pp. 493–495.
18. *Cation distribution and magnetic structure of the ferrimagnetic spinel NiCo₂O₄*. **Marco, José F., et al.** s.l. : Royal Society of Chemistry (RSC), 10 2001, Journal of Materials Chemistry, Vol. 11, pp. 3087–3093.
19. *Cobalt ferrite nanoparticles: Achieving the superparamagnetic limit by chemical reduction*. **Jeppson, P., et al.** s.l. : AIP Publishing, 2006, Journal of Applied Physics, Vol. 100, p. 114324.
20. *Lithium Batteries and Cathode Materials*. **Whittingham, M. Stanley.** s.l. : American Chemical Society (ACS), 10 2004, Chemical Reviews, Vol. 104, pp. 4271–4302.
21. *Valence Change Ability and Geometrical Occupation of Substitution Cations Determine the Pseudocapacitance of Spinel Ferrite XFe₂O₄ (X = Mn, Co, Ni, Fe)*. **Wei, Chao, et al.** s.l. : American Chemical Society (ACS), 6 2016, Chemistry of Materials, Vol. 28, pp. 4129–4133.
22. *Spinel ferrite oxide semiconductor gas sensors*. **Šutka, Andris and Gross, Kārlis A.** s.l. : Elsevier BV, 1 2016, Sensors and Actuators B: Chemical, Vol. 222, pp. 95–105.
23. *Microstructure, mechanical, thermal, {EPR}, and optical properties of {MgAl}₂O₄:Cr³⁺ spinel glass/ceramic nanocomposites*. **Molla, A. R., et al.** s.l. : Elsevier BV, 1 2014, Journal of Alloys and Compounds, Vol. 583, pp. 498–509.
24. *Cleaved cavity optically pumped InGaN–GaN laser grown on spinel substrates*. **Khan, M. Asif, et al.** s.l. : AIP Publishing, 10 1996, Applied Physics Letters, Vol. 69, pp. 2418–2420.
25. *Production of Copper and Cobalt Aluminate Spinel and Their Application As Supports for Inulinase Immobilization*. **Abaide, Ederson Rossi, et al.** s.l. : FapUNIFESP (SciELO), 10 2015, Materials Research, Vol. 18, pp. 1062–1069.
26. *High-performance, transparent conducting oxides based on cadmium stannate*. **Coutts, T. J., et al.** s.l. : Springer Science and Business Media LLC, 6 1996, Journal of Electronic Materials, Vol. 25, pp. 935–943.
27. *Optical and Electrical Properties of Cd₂SnO₄: A Defect Semiconductor*. **Nozik, A. J.** s.l. : American Physical Society (APS), 7 1972, Physical Review B, Vol. 6, pp. 453–459.
28. *Cellulose-precursor synthesis of nanocrystalline Co_{0.5}Cu_{0.5}Fe₂O₄ spinel ferrites*. **(formerly Suriya) Ounnunkad, Kontad and Phanichphant, Sukon.** s.l. : Elsevier BV, 2 2012, Materials Research Bulletin, Vol. 47, pp. 473–477.
29. *High-Q Microwave Dielectric Materials Based on the Spinel Mg₂TiO₄*. **Belous, Anatolii, et al.** s.l. : Wiley, 11 2006, Journal of the American Ceramic Society, Vol. 89, pp. 3441–3445.
30. **Long, G. J. and Grandjean, F.** *Mössbauer Spectroscopy Applied to Inorganic Chemistry*. [ed.] Gary J. Long. s.l. : Springer US, 1984.
31. *The Structure of Magnetite and the Spinel*. **Bragg, W. H.** s.l. : Springer Science and Business Media LLC, 7 1915, Nature, Vol. 95, pp. 561–561.

32. XXX. *The structure of the spinel group of crystals*. **Bragg, W. H.** s.l. : Informa UK Limited, 8 1915, The London, Edinburgh, and Dublin Philosophical Magazine and Journal of Science, Vol. 30, pp. 305–315.
33. *Structure of Some Crystals of Spinel Group*. **Nishikawa, S.** 1915, Proceedings of the Tokyo Mathematico-Physical Society, Vol. 8, pp. 199–209.
34. *Spinel structures: with and without variate atom equipoints*. **Barth, Tom. F. W. and Posnjak, E.** s.l. : Walter de Gruyter GmbH, 1 1932, Zeitschrift für Kristallographie - Crystalline Materials, Vol. 82.
35. *Cation distributions and thermodynamic properties of binary spinel solid solutions*. **O'Neill, H. S. and Navrotsky, A.** 1984, American Mineralogist, Vol. 69, pp. 733–753.
36. *Theoretical Prediction of Structure and Cation Ordering in an Ordered Normal-Inverse Double Spinel, submitted (2020)*. **Pilania, Ghanshyam, et al.** s.l. : Springer Science and Business Media LLC, 11 2020, Comms. Mater., Vol. 1, p. 84.
37. *Unified View of the Local Cation-Ordered State in Inverse Spinel Oxides*. **Liu, Jue, et al.** s.l. : American Chemical Society (ACS), 10 2019, Inorganic Chemistry, Vol. 58, pp. 14389–14402.
38. *Big Data of Materials Science: Critical Role of the Descriptor*. **Ghiringhelli, Luca M., et al.** s.l. : American Physical Society (APS), 3 2015, Physical Review Letters, Vol. 114.
39. *SISSO: A compressed-sensing method for identifying the best low-dimensional descriptor in an immensity of offered candidates*. **Ouyang, Runhai, et al.** s.l. : American Physical Society (APS), 8 2018, Physical Review Materials, Vol. 2.
40. *First-principles study of cation distribution in eighteen closed-shell AIB₂III₂O₄ and AIVB₂II₂O₄ spinel oxides*. **Wei, Su-Huai and Zhang, S.** s.l. : American Physical Society (APS), 1 2001, Physical Review B, Vol. 63.
41. *Diagrammatic Separation of Different Crystal Structures of A₂BX₄ Compounds Without Energy Minimization: A Pseudopotential Orbital Radii Approach*. **Zhang, Xiuwen and Zunger, Alex.** s.l. : Wiley, 5 2010, Advanced Functional Materials, Vol. 20, pp. 1944–1952.
42. *Simple Point-Ion Electrostatic Model Explains the Cation Distribution in Spinel Oxides*. **Stevanović, Vladan, d'Avezac, Mayeul and Zunger, Alex.** s.l. : American Physical Society (APS), 8 2010, Physical Review Letters, Vol. 105.
43. *Ab initio molecular dynamics for liquid metals*. **Kresse, G. and Hafner, J.** s.l. : American Physical Society (APS), 1 1993, Physical Review B, Vol. 47, pp. 558–561.
44. *Ab initio molecular-dynamics simulation of the liquid-metal–amorphous-semiconductor transition in germanium*. **Kresse, G. and Hafner, J.** s.l. : American Physical Society (APS), 5 1994, Physical Review B, Vol. 49, pp. 14251–14269.
45. *Efficient iterative schemes for ab initio total-energy calculations using a plane-wave basis set*. **Kresse, G. and Furthmüller, J.** s.l. : American Physical Society (APS), 10 1996, Physical Review B, Vol. 54, pp. 11169–11186.
46. *Efficiency of ab-initio total energy calculations for metals and semiconductors using a plane-wave basis set*. **Kresse, G. and Furthmüller, J.** s.l. : Elsevier BV, 7 1996, Computational Materials Science, Vol. 6, pp. 15–50.
47. *Generalized Gradient Approximation Made Simple*. **Perdew, John P., Burke, Kieron and Ernzerhof, Matthias.** s.l. : American Physical Society (APS), 10 1996, Physical Review Letters, Vol. 77, pp. 3865–3868.
48. *Projector augmented-wave method*. **Blöchl, P. E.** s.l. : American Physical Society (APS), 12 1994, Physical Review B, Vol. 50, pp. 17953–17979.
49. *From ultrasoft pseudopotentials to the projector augmented-wave method*. **Kresse, G. and Joubert, D.** s.l. : American Physical Society (APS), 1 1999, Physical Review B, Vol. 59, pp. 1758–1775.
50. *Electron-energy-loss spectra and the structural stability of nickel oxide: $\{ \text{LSDA} \} \mathit{+} \mathit{SU}$ study*. **Dudarev, S. L., et al.** s.l. : American Physical Society (APS), 1 1998, Physical Review B, Vol. 57, pp. 1505–1509.
51. *Commentary: The Materials Project: A materials genome approach to accelerating materials innovation*. **Jain, Anubhav, et al.** s.l. : AIP Publishing, 7 2013, APL Materials, Vol. 1, p. 011002.
52. *A fast and robust algorithm for Bader decomposition of charge density*. **Henkelman, Graeme, Arnaldsson, Andri and Jónsson, Hannes.** s.l. : Elsevier BV, 6 2006, Computational Materials Science, Vol. 36, pp. 354–360.
53. *A grid-based Bader analysis algorithm without lattice bias*. **Tang, W., Sanville, E. and Henkelman, G.** s.l. : IOP Publishing, 1 2009, Journal of Physics: Condensed Matter, Vol. 21, p. 084204.
54. *LOBSTER: A tool to extract chemical bonding from plane-wave based DFT*. **Maintz, Stefan, et al.** s.l. : Wiley, 2 2016, Journal of Computational Chemistry, Vol. 37, pp. 1030–1035.
55. *LOBSTER: Local orbital projections, atomic charges, and chemical-bonding analysis from projector-augmented-wave-based density-functional theory*. **Nelson, Ryky, et al.** s.l. : Wiley, 6 2020, Journal of Computational Chemistry, Vol. 41, pp. 1931–1940.
56. *Cation ordering and effect of biaxial strain in double perovskite CsRbCaZnCl₆*. **Pilania, G. and Uberuaga, B. P.** s.l. : AIP Publishing, 3 2015, Journal of Applied Physics, Vol. 117, p. 114103.
57. *Structure maps for. Pseudobinary and ternary phases*. **Pettifor, D. G.** s.l. : Informa UK Limited, 8 1988, Materials Science and Technology, Vol. 4, pp. 675–691.
58. *Thermodynamics of formation of simple spinels*. **Navrotsky, A. and Kleppa, O. J.** s.l. : Elsevier BV, 2 1968, Journal of Inorganic and Nuclear Chemistry, Vol. 30, pp. 479–498.
59. *Interaction of cations on octahedral and tetrahedral sites in simple spinels: A reply*. **Urusov, V. S.** s.l. : Springer Science and

ARTICLE

Journal Name

Business Media LLC, 3 1984, *Physics and Chemistry of Minerals*, Vol. 10, pp. 194–195.

60. *Octahedral site preference energy*. **Reznitskii, L. A.** 1976, *Izv Akad Nauk SSSR Neorg Mater.*

61. *Structure of Spinel*. **Sickafus, Kurt E., Wills, John M. and Grimes, Norman W.** s.l. : Wiley, 12 2004, *Journal of the American Ceramic Society*, Vol. 82, pp. 3279–3292.

62. *Relationship between Average Cation Radii and Oxygen Parameter for Various Oxides with Spinel-Type Structure*. **Yokoyama, Takashi and Meguro, Takeshi.** s.l. : IOP Publishing, 8 2005, *Japanese Journal of Applied Physics*, Vol. 44, pp. 6201–6203.

63. *Artificial intelligence for high-throughput discovery of topological insulators: The example of alloyed tetradymites*. **Cao, Guohua, et al.** s.l. : American Physical Society (APS), 3 2020, *Physical Review Materials*, Vol. 4.

64. *Functional form of the superconducting critical temperature from machine learning*. **Xie, S. R., et al.** s.l. : American Physical Society (APS), 11 2019, *Physical Review B*, Vol. 100.

65. *Machine-Learning-Based Predictive Modeling of Glass Transition Temperatures: A Case of Polyhydroxyalkanoate Homopolymers and Copolymers*. **Pilania, Ghanshyam, et al.** s.l. : American Chemical Society (ACS), 11 2019, *Journal of Chemical Information and Modeling*, Vol. 59, pp. 5013–5025.

66. *New tolerance factor to predict the stability of perovskite oxides and halides*. **Bartel, Christopher J., et al.** s.l. : American Association for the Advancement of Science (AAAS), 2 2019, *Science Advances*, Vol. 5, p. eaav0693.